# Wavelet-based decomposition of the tonal-broadband components of propeller noise

Meloni, S; de Paola, E. ; Grande, E.; Ragni, D.; Stoica, L. G. ; Di Marco, A. ; Camussi, R.

# Wavelet-based decomposition of the tonal-broadband components of propeller noise

S. Meloni [*] and E. de Paola [†]

*Roma Tre University, Department of Engineering, Via Vito Volterra, 62, 00146 Rome (Itay)*

E. Grande [‡] and D. Ragni[§]

*Faculty of Aerospace Engineering, Delft University of Technology, Kluyverweg 1, 2629 HS Delft, The Netherlands*

L. G. Stoica[¶], A. Di Marco[‖], and R. Camussi[**]

*Roma Tre University, Department of Engineering, Via Vito Volterra, 62, 00146 Rome (Itay)*

**The present study reports a novel wavelet-based method aimed at separating the noise emitted by a single propeller into two contributions, tonal and broadband. An assessment using two different experimental investigations of propellers operating in diverse configurations is presented. The first experiment focuses upon near-field polar microphone array data of a benchmarked low-Reynolds number propeller, in hover and cruise conditions. Measurements were performed in the anechoic tunnel (A-Tunnel) at the low-speed laboratory of TU Delft. The second set of data consists of a test campaign carried out at the Pininfarina Aerodynamic and Aeroacoustic Research Center in Turin (Italy) under the EU funded project ERaCLE. The model comprises a five-bladed propeller installed close to a wing. Pressure signals were acquired using a top-mounted linear microphone array that spans different polar locations. The wavelet-based algorithm able to separate the tonal and broadband contributions through the computation of two-point statistics. The assessment of the decomposition procedure on two very different databases is presented to validate the technique with the aim to extend its range of applications.**

## I. Nomenclature

| | | |
|---|---|---|
| $x$ | = | axial coordinate |
| $y$ | = | radial coordinate |
| $z$ | = | radial coordinate |
| $RPM$ | = | propeller speed expressed in revolutions per minute |
| $U$ | = | wind tunnel velocity, m s$^{-1}$ |
| $w(s,t)$ | = | wavelet coefficients |
| $D$ | = | propeller diameter |
| $p_o$ | = | original signal |
| $p_t$ | = | tonal component |
| $p_{blf}$ | = | low frequency broadband component |
| $p_{bts}$ | = | broadband component after the tresholding procedure |
| $p_b$ | = | whole broadband component |
| $\theta_m$ | = | microphone polar angle, ° |
| $SPL$ | = | sound pressure level |
| $PSD$ | = | power spectral density |

---

[*]Research Fellow, Roma Tre University, Department of Engineering, stefano.meloni@uniroma3.it

[†]Research Fellow, Roma Tre University, Department of Engineering.

[‡]PhD student, Faculty of Aerospace Engineering, Delft University of Technology.

[§]Associate Professor, Faculty of Aerospace Engineering, Delft University of Technology.

[¶]PhD student, Roma Tre University, Department of Engineering.

[‖]Research assistant, Roma Tre University, Department of Engineering.

[**]Full Professor, Roma Tre University, Department of Engineering.

| $P_{ref}$ | = | reference pressure in air |
| $T$ | = | threshold level |
| $J$ | = | advance ratio |

## II. Introduction

Increasing concerns about the environment resulted in the need for innovative design solutions, with the aim to improve the fuel efficiency of conventional aircraft configurations. This has led the industry and the scientific community to focus their attention on propellers as an alternative to turbofan engines. As a consequence, recent interest in hybrid-electric [1] and fully-electric [2] propulsion made the concept of distributed electric propulsion (DEP) even more attractive. In addition, advances in non-expensive electronic control systems and propulsive devices promoted the development and deployment of small Unmanned Aerial Vehicles (UAVs) in a wide variety of applications. Owing to their hovering ability, vertical take-off and landing, and user-friendly flight controllability, UAVs with multi-rotor systems are becoming very popular among the engineering community, with the consequent need for noise reduction methods. Many noise sources contribute to the noise emissions from unmanned aerial systems, [3, 4], but none of them is as significant as the propeller noise [5–7]. Despite many improvements have been achieved in rotor design, installed propeller noise emissions remain a challenging topic.

The sound radiated by rotating systems such as propellers, fans and rotors, has a variety of tonal, narrow-band and broadband components [8, 9]. The richness and the complexity of this sound radiation makes the study of such systems both scientifically and technologically demanding. To develop reliable noise reduction strategies, it is necessary to separate and understand the noise generation mechanisms involved with these systems and the physics associated with each noise source. Brooks et al.[10] identified the major tonal and broadband noise sources of a propeller in a classical configuration as: (1) the tonal self-noise, which is generated by the volume displacement and the aerodynamic loading on the surface of the blade; (2) blade-vortex interaction (BVI) noise, which occurs when the blade tip vortex impinges on a subsequent blade; (3) blade-wake interaction (BWI) noise, which occurs when the turbulent wake formed behind a blade impinges on a subsequent blade; and (4) broadband self-noise, which is due to the interaction between the blade trailing edge and the turbulent boundary layer.

The knowledge of individual noise levels of tone and broadband plays an important role in many noise reduction investigations. Thus, the determination of the single noise contributions becomes very important for properly assessing the noise control parameters and for validating open rotor noise simulation codes [8, 11]. A signal processing technique was developed by Sree [12] to separate the tonal and broadband noise components from open rotor acoustic data. To assess its reliability, the technique was applied to simulated data as well as experimental acoustic data generated from a hobby-aircraft open rotor. Although a partial separation of the energy of the signal into tonal and broadband noise components was achieved in these two cases, the technique did not account for the random phase shifts occurring in the long data segment-pairs selected for the cross-correlation operation. This implies that non-trivial tonal content still could be found in the broadband spectrum. In the study, therefore, the actual acoustic power pertaining to the solely tonal and broadband components could not be properly quantified. A deeper description of the limitations of this technique is discussed by Sree [12], and Sree and Stephens [13]. A new method for processing open rotor data capable to minimize the effects of phase shifts, and thereby eliminating the spike levels in the broadband spectrum, was later presented by Sree and Stephens [14], as an improved algorithm of the original technique. This method was found to reliably perform with data from both single-shaft turbofan models and two-shaft counter-rotating propeller models running at the same rotational speed. A further study revealed that the technique outperforms the classical peak detection approach, in separating the tone and broadband components [15]. Peak detection algorithms are inherently user-input-driven, requiring either an expected spectral shape, peak height threshold, or other smoothing parameters. The user typically runs them multiple times, comparing the results against their expectations. This led to the need for a more robust approach to separate the noise into its components, which is not affected by the user's choices and is applicable to the more general case of operating rotors. In this paper, a new wavelet-based algorithm is presented to separate the tonal and broadband components in the noise signal emitted by single propeller configurations operating at different Reynolds number. The focus of this work is the assessment of the presented procedure on databases constituted by configurations of propulsive systems under several flight conditions and scientifically interesting in light of the application of both UAV systems and DEP configurations. The first test-case, corresponds to the pressure field from a bench-marked low-Reynolds number propeller (Re $\approx 10^4$) tested at the TU Delft low-speed laboratory, in the anechoic A-tunnel. Data have been acquired at different advance ratios using a near field array of microphones positioned at 4 diameters from the propeller disc plane.

The second database, from the ERaCLE EU funded project through the H2020 Clean Sky program, contains measurements achieved in the Pininfarina Aerodynamic and Aeroacoustic Research Center in Turin, Italy. The model tested consists of an installed propeller-wing configuration characterised by a Reynolds number of about $10^6$. The wing employs a NACA 0015 airfoil, coupled with a 5-bladed propeller having an adjustable pitch angle. The use of data obtained in very different configurations and in diverse facilities allows us to provide a robust assessment of the decomposition procedure generalizing its suitability to a wide range of applications in propeller aeroacoustics. The paper is structured as follows. Key information about the experiments conducted to generate the datasets used are presented in section II. In Sect. III we reported details about the wavelet decomposition algorithm, and results are reported in Section IV. Conclusions and proposals for the full-length paper are reported in section V.

## III. Experimental setups

### A. Low-Reynolds number propeller

The experiments have been carried out in the anechoic tunnel (A-tunnel), located at the low-speed laboratory of TU Delft. The A-tunnel is a vertical, open-jet wind tunnel, installed in an anechoic chamber with walls covered by melamine wedges [16]. A circular exit nozzle with a diameter of 0.60 m and a contraction ratio of 15:1 has been employed for this study. The propeller used for this investigation is a benchmarked version obtained from an APC 9x6 blade, with a diameter of 22.86 cm and a pitch of 15.24 cm. The diameter has been scaled up to D=30 cm and each profile has been reshaped with an NACA 4412 airfoil (see [17]). The propeller, made of an aluminium alloy, has been manufactured using computer numerical control machining at TU Delft with 0.4 to 0.8$\mu$m Ra finish. This manufacturing method guarantees high accuracy and minimizes the surface imperfections, which can induce vibrations during the measurements and can affect the quality of the flow around the blades. The propeller is connected to a profiled aluminium nacelle of 5 cm diameter for minimum interference with the propeller flow. Within the nacelle, a motor, an encoder, a load cell, and a torque cell are assembled. The nacelle is supported by stiffened hollow aluminum NACA 0012 profiles of 6 cm chord, inside which all the cabling are housed and remotely connected to the instrumentation outside the jet. The entire structure is held up above the nozzle of the tunnel by four steel-wire tubes of 2 cm diameter fixed to the tunnel to minimize vibrations and interference. The propeller is driven by an electric brushless motor, Leopard Hobby 3536-5T 1520 KV, with a diameter of 27.8 mm and a maximum power of 550 W. The motor is powered by a Delta Elektronika DC power supply with a voltage range of 0–15 V and a current range of 0–100 A. The motor rotational speed is measured using a US Digital EM1 transmissive optical encoder, coupled with a US Digital disk of 25.4 mm diameter and 200 cycles per revolution (1.8 deg of uncertainty on the position).

The microphone array is constituted by 13 G.R.A.S. 40PH analogue free-field microphones, having a diameter of 7 mm, a frequency range between 10 and 20 KHz, and a maximum sound pressure level (SPL) of 135 dB. The microphones are calibrated using a G.R.A.S. 42AA piston-phone with a 250 Hz pressure wave having an amplitude of 114 dB (reference sound pressure of 20$\mu Pa$). The uncertainty of the calibration is less than 0.09 dB (99 confidence level). The data acquisition system consists of a National Instrument PXIe-4499 sound and vibrations data acquisition module. The distance between each microphone is 0.5D (0.15 m), microphone 7 is at the propeller plane, microphone 1 is 3D (0.9 m) above the propeller plane, and microphone 13 is 3D below. Microphone voltages have been recorded for a duration of 30 s at a frequency rate of 50 kHz. A photograph of the experimental setup and a schematic of the propeller are reported in figure 1 (a) and (b) respectively.

### B. Installed pusher propeller

The test campaign was carried out at the Pininfarina Aerodynamic and Aeroacoustic Research Center in Turin, Italy. The semi-cylindrical open-jet wind tunnel, driven by a 29-bladed fan, is characterised by having a collector of 3 m radius and a test section of 8 m x 9.6 m x 4.2 m. An appropriate acoustic treatment of the wind tunnel reduces the background noise to 68.5 dBA at a flow velocity of 28 m/s and 77.7 dBA at 39 m/s, measured out of the flow. The tunnel produces a uniform velocity flow, which varies by only 0.5% over the area of the test section with a turbulence intensity controlled between 0.26-8%. The wing employs a NACA 0015 airfoil; the angle of attack of the entire model varies by means of a turntable mounted on the WT ground. Each propeller has 5 blades, with an adjustable pitch angle, rotating in counterclockwise direction, looking upstream. The electric motors which power the propellers are provided with an air cooling system to control their operating temperature.

The reference system is centred at mid-width of the open jet nozzle exit plane. Far field sound measurements were
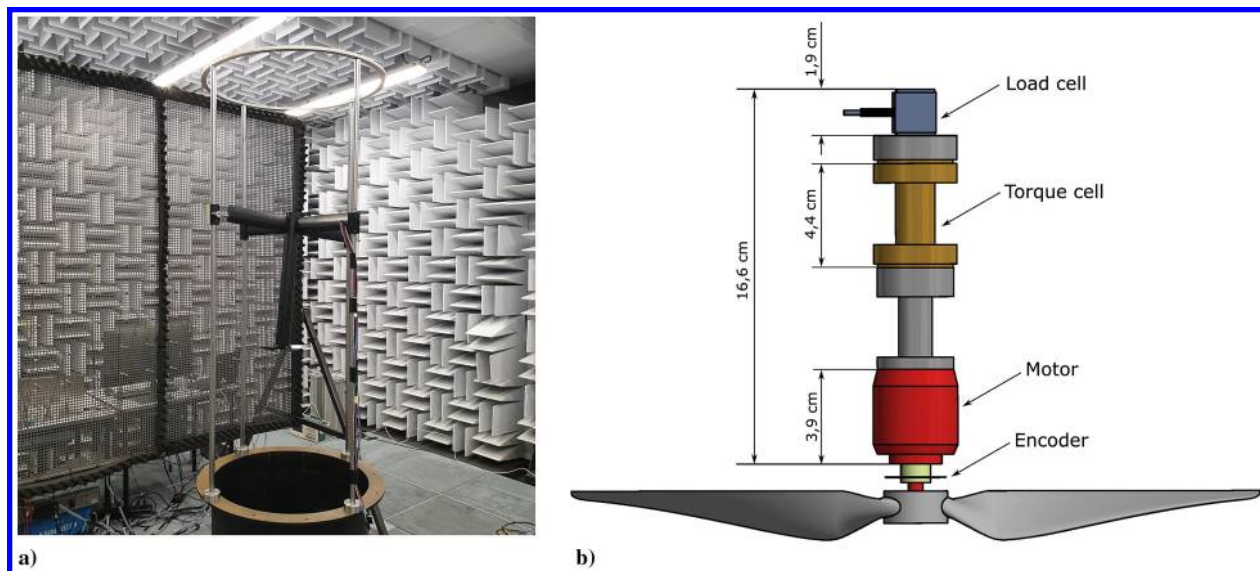
**Fig. 1    a) A photograph of the experimental setup mounted in the A-tunnel; b) A schematic view of the propeller drive train;**
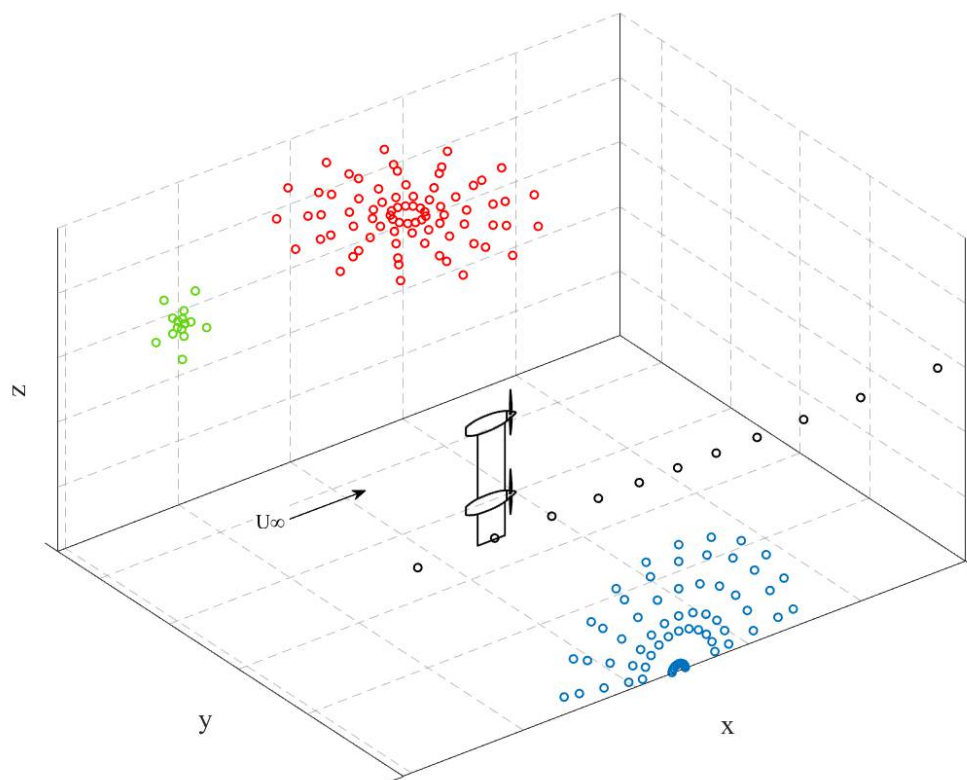


**Fig. 2    Set- up ERaCLE.**

performed using 4 microphone arrays: a top, a lateral, a front and linear array. Their positions are shown in Figure 2 together with a sketch of the model and its position with respect to the jet flow.

The linear array of 11 B&K 4189 type microphones is centred on the propellers plane in baseline configuration and each sensor is directed towards a point midway between the two rotors. The linear array covers measured angles from approximately 40° to 140° calculated with respect to the focal point. The layout of this array is shown by the black dots in figure 2 and sensor coordinates are provided in Table 1. All the microphone arrays are positioned outside the WT flow. In the single propeller tests, the relative distance between the propellers is fixed at $\Delta z/D = 1.60$, while the axial distance with respect to the wing is in the baseline position. The helical tip Mach number is set to 0.26, resulting from the rotational speed and wind tunnel speed at a constant value of the advance ratio $J = 1.12$. The algorithm is only applied to the data acquired at 0° angle of attack, and at a fixed blade pitch angle.

| Mic number | 1 | 2 | 3 | 4 | 5 | 6 | 7 | 8 | 9 | 10 | 11 |
|---|---|---|---|---|---|---|---|---|---|---|---|
| X/D | 0.78 | 2.55 | 3.85 | 4.92 | 5.85 | 6.75 | 7.62 | 8.56 | 9.63 | 10.9 | 12.7 |
| Y/D | -6.15 | -6.15 | -6.15 | -6.15 | -6.15 | -6.15 | -6.15 | -6.15 | -6.15 | -6.15 | -6.15 |
| Z/D | 3.6 | 3.6 | 3.6 | 3.6 | 3.6 | 3.6 | 3.6 | 3.6 | 3.6 | 3.6 | 3.6 |
| $\theta_m$ [°] | 40 | 50 | 60 | 70 | 80 | 90 | 100 | 110 | 120 | 130 | 140 |

**Table 1    Microphone linear array: coordinates and angles with respect to the propeller plane.**

## IV. Tonal-Broadband decomposition methodology

The wavelet transform is a suitable tool when it comes to analyzing localized events, allowing the simultaneous representation of a temporal signal in terms of a time shift (t) and a resolution time scale (s) which inversely corresponds to the frequency (f) [18–21]. The wavelet approach is based on the projection of the acquired signal onto the basis of compact support functions localized both in the time domain and in the transformed space. Formally, the wavelet transform of the propeller pressure signal p(t) is given by the following expression:

$$w(s,t) = C_\psi^{\frac{-1}{2}} s^{\frac{-1}{2}} \int_{-\infty}^{\infty} p(\tau)\psi^*\left(\frac{\tau-t}{s}\right)d\tau, \tag{1}$$

where $s$ is the wavelet scale , $\tau$ is a time shift, $C_\psi^{\frac{-1}{2}}$ is a constant that takes into account the mean value of $\psi(t)$ and $\psi^*\left(\frac{t-\tau}{s}\right)$ is the complex conjugate of the dilated and translated mother wavelet $\psi(t)$.

The decomposition procedure presented in this work is based on the discrete wavelet transform (DWT), which uses as a support function a discrete mother wavelet and is a well-assessed alternative to the Fast Fourier transform (FFT) [20]. For this kind of application, the mother wavelet selection is not trivial due to the presence of pseudo periodic oscillatory features. According to biomedical experiences (see e.g. [22–24]) in the denoising of electrocardiogram (ECG) signals, which are also characterized by regular tones, the authors used for this application a Symlets mother wavelet [22]. This nearly symmetric mother wavelet could exhibit different vanishing moments, which value has been selected for this decomposition procedure at 6 (i.e. Sym6). Furthermore, signals have been filtered using a high-frequency bandpass filter to avoid low-frequency spurious effects.

Filtered signals have been inserted into an iterative denoising algorithm based, as aforementioned, on the discrete wavelet transform. The iterative procedure follows what is reported in [20, 25], and enables us to separate the wavelet coefficients into two sets: in this case, we assume that coefficients above the threshold are related to the tonal signatures and those having magnitude lower than the threshold we considered representative of the broadband region. Thanks to the orthogonality of the wavelet base adopted, the two wavelet sets can be inverse-transformed to reconstruct the two split counterparts in the physical space as two distinct signals.

$$p_o = p_t + p_b, \tag{2}$$

where $p_t$ it the tonal counterpart, $p_{b'}$ the broadband signal obtained after the iterative procedure. The trick of this method is based on the definition of the thresholding procedure. For this analysis we define the threshold level in a similar way to [25, 26], thus as,

$$T = \sqrt{2p_b'|_k log_{10}N_s}, \tag{3}$$

where $p_{p'}'$ is the variance of the signal counterpart related to the broadband region, $N_s$ is the number of samples, and k identifies each iteration. In the first iteration, the variance of the original signal has been used. The threshold is

5

discretely changed until a proper convergence criterion, capturing the different nature of the separated signals. Two different convergence criteria were considered for these cases, both based on the cross-correlation:

$$max(\rho_b)_{(it-1)} - max((\rho_b)_{(it)} < err. \tag{4}$$

This criterion, as reported in eq 4, stops the algorithm when the cross-correlation peak of the broadband component does not vary between two consecutive iterations. This is the criterion applied for the results presented in this extended abstract. The second criterion is based on the cross correlation of the tonal counterpart:

$$mean(peaks(\rho_t))_{(it-1)} - mean(peaks((\rho_t))_{(it)} < err, \tag{5}$$

thus stopping the code when the average value of the tonal component cross-correlation peaks does not vary between two consecutive iterations. The two criteria compared by the authors produced the same result.

By the end, as aforementioned, the entire broadband and tonal signals have been reconstructed using the inverse wavelet transform and analyzed in the following chapter for the presented configurations.

## V. Results

As anticipated, the procedure has been assessed considering two different databases, the first one has been carried out at the university of TU Delft and it is based on a low-Reynolds number propeller, whereas the second one considers a pushing propeller system and has been conducted under ERaCLE Clean Sky European project. In the following paragraphs the details about the results can be found.

### A. Low-Reynolds number propeller

Results from the wavelet decomposition procedure applications on signals acquired slightly downstream of the propeller disc plane are presented in terms of SPL evaluated as:

$$SPL = 10 \log_{10}\left(\frac{\text{PSD}\Delta f_{\text{ref}}}{P_{\text{ref}}^2}\right), \tag{6}$$

where PSD denotes the power spectral density evaluated using Welch's method, $\Delta f_{\text{ref}}$ is the frequency bandwidth and $P_{\text{ref}}$ is the reference pressure in air (equal to $20\mu$Pa). Spectra were reported in Figure 3(a) and (c) in hover and with an advance ratio of J=0.4 respectively. We observed that the decomposition method in both cases well separated the tonal peaks related to the blade passage from the broadband region of the entire spectrum.

The effect of the decomposition has been also checked in the time domain through the cross-correlation function defined as:

$$R_{i,i+1} = < p(x,t), p(x+\xi, t+\tau) >, \tag{7}$$

where $\xi$ is the distance in the polar direction between the two consecutive microphones, $\tau$ is the time lag and the symbol $<>$ denotes a time average. The cross-correlations coefficients $\rho_{i,i+1}$, obtained normalizing $R_{i,i+1}$ by the product of the standard deviations of the two pressure signals. Cross correlations were reported in figure 3(b) and (d) for the low-Reynolds number propeller configuration. The broadband component ($p_b$) of the cross-correlation in both cases results smoothly with no harmonic effects generated by the blade passing frequency. These periodic oscillations result in higher in the tonal counterpart if compared with the original signal because of the removal of the broadband component. The presence of the advance ratio seems to mask the harmonic oscillations in the original cross-correlation, which instead are well visible in the tonal counterpart(see fig. 3 (d)).

### B. Installed pusher propellers

In this paragraph, an assessment of the decomposition method of the noise emitted by a propeller-wing configuration is carried out. As for the previous paragraph, results are presented in terms of spectra and cross-correlations. We plot results versus non-dimensional frequency, obtained normalising by the blade passing frequency (BPF). The configuration under study is the installed single inboard propeller which is interacting with the wing throughout its entire diameter. As expected, the tonal noise produced by the rotor is predominant at the BPF harmonics, however, two considerations must be taken into account: the low frequency range is influenced by wind tunnel flow effects and the harmonic content
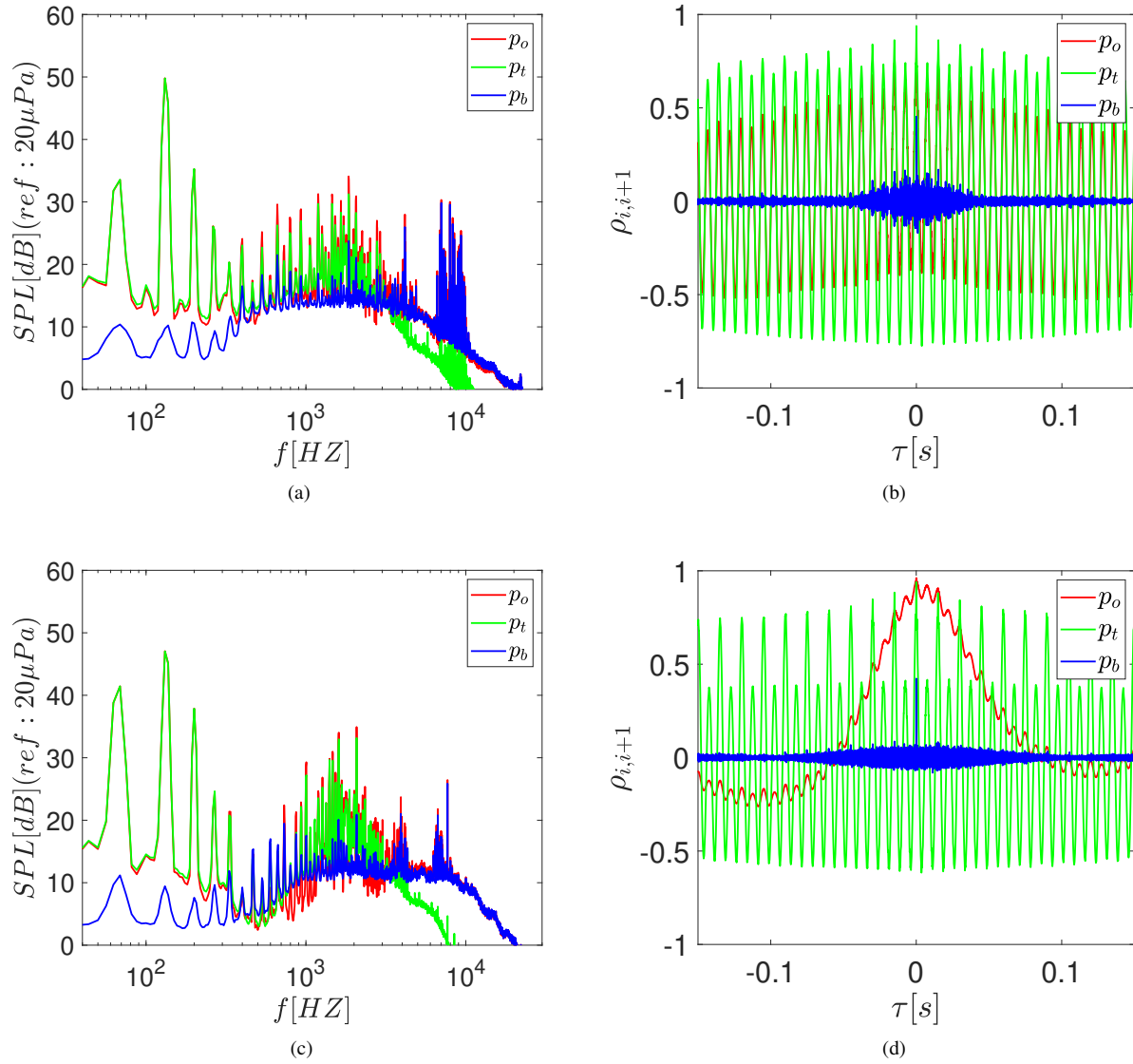
**Fig. 3    a) SPL of a microphone positioned close to the propeller disk plane, in hover; b) Cross-Correlation between two consecutive microphones in the same position of a). Figures (c) and (d) report the same plot with an advance ratio of J=0.4**

of the tunnel fan, characterised by a BPF of about one third of that of the propeller, is also found in the spectrum. The decomposed spectra reported in Figure 4 (a) show quite a good separation of the proposed contributions.

In addition, for this configuration, the cross-correlation of the separated tonal counterpart perfectly shows the expected pseudo-periodic trend, although the original signal appears to be very smooth, without any apparent harmonic effect generated by the blade passage.

## VI. Conclusion

This work brings forward a novel approach to decomposing the noise emitted by a single propeller using a wavelet-based technique in tonal and broadband counterparts. Unlike previous studies, the presented method can reconstruct both tonal and broadband time series, which could be used to evaluate the different physical characteristics of the two noise phenomena. An algorithm assessment using two databases gained in various facilities has been reported,
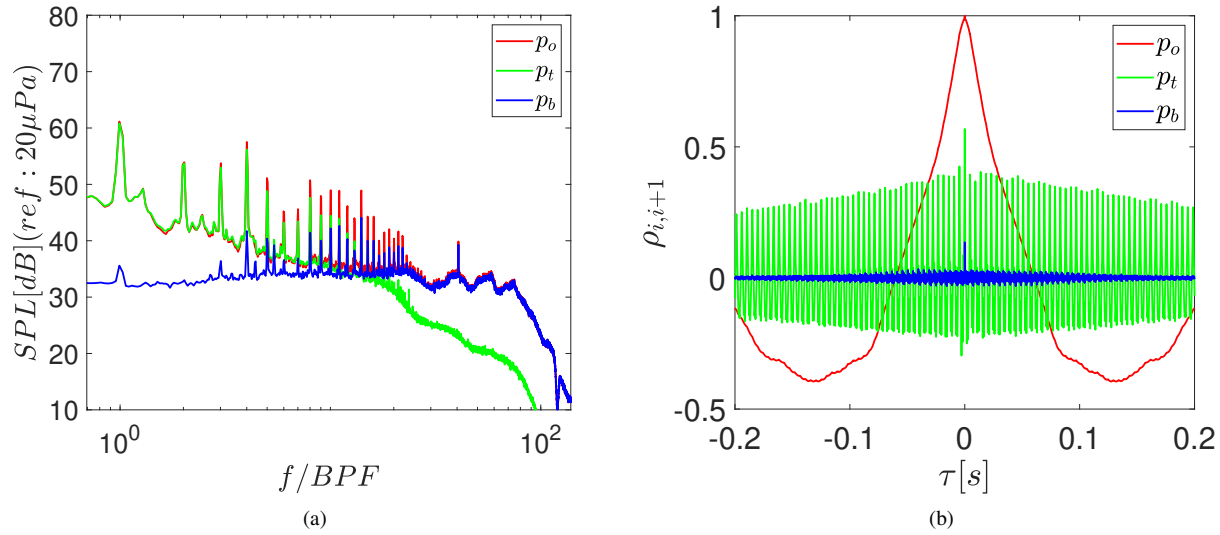
**Fig. 4    a) SPL of a microphone positioned close to the propeller disk plane, at a Reynolds number Re=3.6 · 10⁶ and an advance ratio of J=1.12; b) Cross-Correlation between two consecutive microphones in the same zone.**

observing that the algorithm can robustly separate the noise contributions with no specific inputs from the user for a wide range of applications. Furthermore, the cross-correlation functions highlighted more evident oscillatory pseudo periodic trends in the tonal part with respect to the original signal; this is more evident with advancing propeller configurations, where the BPF oscillations are masked in the acquired times series cross-correlation by different broadband effects. In conclusion, this first application of the wavelet transforms on separating the two components that characterize the propeller noise shows that this approach could be a very efficient tool. However, further analyses of the algorithm's sensibility and applications are needed to provide a complete assessment.

## Acknowledgments

## References

[1] Friedrich, C., and Robertson, P. A., "Hybrid-Electric Propulsion for Aircraft," *Journal of Aircraft*, Vol. 52, No. 1, 2015, pp. 176–189. doi:10.2514/1.C032660, URL https://doi.org/10.2514/1.C032660.

[2] Moore, M. D., "Misconceptions of Electric Aircraft and their Emerging Aviation Markets," *52nd Aerospace Sciences Meeting*, 2014. doi:10.2514/6.2014-0535, URL https://arc.aiaa.org/doi/abs/10.2514/6.2014-0535.

[3] Dahan, C., Avezard, L., and Guillien, G., *Propeller light aircraft noise at discrete frequencies*, Journal of Aircraft, Vol. 18, No. 6, pp. 480-486, 1980.

[4] Massey, K., and Gaeta, R., *Noise measurements of tactical UAVs*, AIAA Paper 2010-3911, 2010.

[5] Sinibaldi, G., and Marino, L., *Experimental analysis on the noise of propellers for small UAV*, Applied Acoustics, Vol. 74, No. 1, pp. 79-88, 2013.

[6] Intaratep, N., Alexander, N., W., Devenport, J., W., Grace, M., S., and Dropkin, A., *Experimental study of quadcopter acoustics and performance at static thrust conditions*, AIAA Paper 2016-2973, 2016.

[7] Christian, A. W., D., B. D., Zawodny, ., N. S, and Rizzi, S. A., *Auralization of tonal rotor noise components of a quadcopter flyover*, InterNoise, 2015.

[8] Hubbard, H. H., "Aeroacoustics of Flight Vehicles: Theory and Practice," 1994.

[9] Smith, M. J. T., *Aircraft Noise*, Cambridge Aerospace Series, Cambridge University Press, 1989. doi:10.1017/CBO9780511584527.

[10] Brooks, T. F., Jolly, R., and Marcolini, M., *Helicopter main-rotor noise: determination of source contribution using scaled model data*, Tech. Rep. TP 2825 NASA, 1988.

[11] Blandeau, V. P., and Joseph, P. F., "Broadband Noise Due to Rotor-Wake/Rotor Interaction in Contra-Rotating Open Rotors," *AIAA Journal*, Vol. 48, No. 11, 2010, pp. 2674–2686. doi:10.2514/1.J050566, URL https://doi.org/10.2514/1.J050566.

[12] Sree, D., "A Novel Signal Processing Technique for Separating Tonal and Broadband Noise Components from Counter-Rotating Open-Rotor Acoustic Data," *International Journal of Aeroacoustics*, Vol. 12, No. 1-2, 2013, pp. 169–188. doi:10.1260/1475-472X.12.1-2.169, URL https://doi.org/10.1260/1475-472X.12.1-2.169.

[13] Stephens, D., and Sree, D., "Tone and Broadband Noise Separation from Acoustic Data of a Scale-Model Counter-Rotating Open Rotor," *20th AIAA/CEAS Aeroacoustics Conference*, 2014. URL https://arc.aiaa.org/doi/abs/10.2514/6.2014-2744.

[14] Sree, D., and Stephens, B., D., "Improved Separation of Tone and Broadband Noise Components from Open Rotor Acoustic Data," *Aerospace*, Vol. 3, No. 3, 2016. doi:10.3390/aerospace3030029, URL https://www.mdpi.com/2226-4310/3/3/29.

[15] Kingan, M., Blandeau, V., Tester, B., Joseph, P., and Parry, A., "Relative importance of open rotor tone and broadband noise sources," *17th AIAA/CEAS Aeroacoustics Conference (32nd AIAA Aeroacoustics Conference)*, 2012. URL https://arc.aiaa.org/doi/abs/10.2514/6.2011-2763.

[16] Merino-Martínez, R., Rubio Carpio, A., Lima Pereira, L. T., van Herk, S., Avallone, F., Ragni, D., and Kotsonis, M., "Aeroacoustic design and characterization of the 3D-printed, open-jet, anechoic wind tunnel of Delft University of Technology," *Applied Acoustics*, Vol. 170, 2020, p. 107504. doi:https://doi.org/10.1016/j.apacoust.2020.107504, URL https://www.sciencedirect.com/science/article/pii/S0003682X20306083.

[17] Grande, E., Romani, G., Ragni, D., Avallone, F., and Casalino, D., "Aeroacoustic Investigation of a Propeller Operating at Low Reynolds Numbers," *AIAA Journal*, Vol. 0, No. 0, 0, pp. 1–12. doi:10.2514/1.J060611, URL https://doi.org/10.2514/1.J060611.

[18] Farge, M., Schneider, K., Pellegrino, G., Wray, A. A., and Rogallo, R. S., "Coherent vortex extraction in three-dimensional homogeneous turbulence: Comparison between CVS-wavelet and POD-Fourier decompositions," *Physics of Fluids*, Vol. 15, No. 10, 2003, pp. 2886–2896. doi:10.1063/1.1599857, URL https://aip.scitation.org/doi/abs/10.1063/1.1599857.

[19] Meloni, S., Lawrence, J. L., Proenca, A. R., Self, R. H., and Camussi, R., "Wall pressure fluctuations induced by a single stream jet over a semi-finite plate," *International Journal of Aeroacoustics*, Vol. 0, No. 0, 2020, p. 1475472X20930650. doi:10.1177/1475472X20930650, URL https://doi.org/10.1177/1475472X20930650.

[20] Camussi, R., and Meloni, S., "On the Application of Wavelet Transform in Jet Aeroacoustics," *Fluids*, Vol. 6, No. 8, 2021. doi:10.3390/fluids6080299, URL https://www.mdpi.com/2311-5521/6/8/299.

[21] Meloni, S., and Kamliya Jawahar, H., "A Wavelet-Based Time-Frequency Analysis on the Supersonic Jet Noise Features with Chevrons," *Fluids*, Vol. 7, No. 3, 2022. doi:10.3390/fluids7030108, URL https://www.mdpi.com/2311-5521/7/3/108.

[22] Li, W., "Wavelets for Electrocardiogram: Overview and Taxonomy," *IEEE Access*, Vol. 7, 2019, pp. 25627–25649. doi:10.1109/ACCESS.2018.2877793.

[23] Lin, H.-Y., Liang, S.-Y., Ho, Y.-L., Lin, Y.-H., and Ma, H.-P., "Discrete-wavelet-transform-based noise removal and feature extraction for ECG signals," *IRBM*, Vol. 35, No. 6, 2014, pp. 351–361. doi:https://doi.org/10.1016/j.irbm.2014.10.004, URL https://www.sciencedirect.com/science/article/pii/S1959031814001298, healthcom 2013.

[24] Smith, C., Agaian, S., and Akopian, D., "A Wavelet-Denoising Approach Using Polynomial Threshold Operators," *IEEE Signal Processing Letters*, Vol. 15, 2008, pp. 906–909. doi:10.1109/LSP.2008.2001815.

[25]  Ruppert-Felsot, J., Farge, M., and Petitjeans, P., "Wavelet tools to study intermittency: application to vortex bursting," *Journal of Fluid Mechanics*, Vol. 636, 2009, p. 427–453. doi:10.1017/S0022112009008003.

[26]  Donoho, D. L., and Johnstone, I. M., "Ideal spatial adaptation by wavelet shrinkage," *Biometrika*, Vol. 81, No. 3, 1994, pp. 425–455. doi:10.1093/biomet/81.3.425.